

# Enhanced Piezoelectricity and Stretchability in Energy Harvesting Devices Fabricated from Buckled PZT Ribbons

Yi Qi,<sup>†</sup> Jihoon Kim,<sup>†</sup> Thanh D. Nguyen,<sup>†</sup> Bozhena Lisko,<sup>†</sup> Prashant K. Purohit,<sup>\*,†</sup> and Michael C. McAlpine<sup>\*,†</sup>

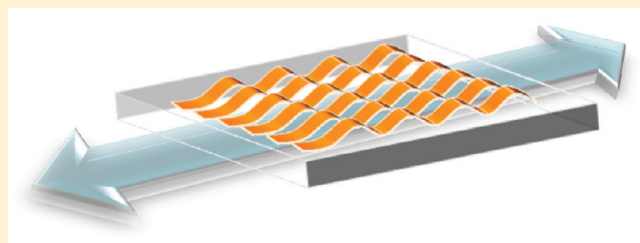
<sup>†</sup>Department of Mechanical and Aerospace Engineering, Princeton University, Princeton, New Jersey 08544, United States

<sup>‡</sup>Department of Mechanical Engineering and Applied Mechanics, University of Pennsylvania, Philadelphia, Pennsylvania 19104, United States

**S** Supporting Information

**ABSTRACT:** The development of a method for integrating highly efficient energy conversion materials onto soft, biocompatible substrates could yield breakthroughs in implantable or wearable energy harvesting systems. Of particular interest are devices which can conform to irregular, curved surfaces, and operate in vital environments that may involve both flexing and stretching modes. Previous studies have shown significant advances in the integration of highly efficient piezoelectric nanocrystals on flexible and bendable substrates. Yet, such inorganic nanomaterials are mechanically incompatible with the extreme elasticity of elastomeric substrates. Here, we present a novel strategy for overcoming these limitations, by generating wavy piezoelectric ribbons on silicone rubber. Our results show that the amplitudes in the waves accommodate order-of-magnitude increases in maximum tensile strain without fracture. Further, local probing of the buckled ribbons reveals an enhancement in the piezoelectric effect of up to 70%, thus representing the highest reported piezoelectric response on a stretchable medium. These results allow for the integration of energy conversion devices which operate in stretching mode via reversible deformations in the wavy/buckled ribbons.

**KEYWORDS:** Hybrid nanomechanics, flexoelectric effect, stretchable energy harvesting, piezoribbons



Biomechanical energy represents a feasible source of continuous power for wearable or implantable devices.<sup>1–7</sup> Since such applications operate via strain-driven modes, they require the associated energy converting devices to be both flexible and stretchable. Recent research has accelerated in the implementation of highly efficient nanoscale piezoelectric energy harvesters on unconventional substrates and in unusual form factors for bendable energy harvesting.<sup>2,3,5,6,8</sup> Yet, stretchability remains a more difficult prospect, as the strains involved can exceed the fracture limits of the most efficient piezoelectric crystals. Polymeric polyvinylidene fluoride (PVDF) nanofibers are naturally flexible and stretchable, accommodating a maximal strain of 2% or higher.<sup>9</sup> However, this advantage is offset by the relatively weak electromechanical coupling, with a piezoelectric coefficient of  $-25$  pC/N.<sup>10</sup> On the other hand, most highly efficient piezoelectric inorganic ceramic materials are mechanically brittle. For example, lead zirconate titanate (PZT,  $\text{Pb}[\text{Zr}_{0.52}\text{Ti}_{0.48}]\text{O}_3$ ) has a piezoelectric coefficient  $\sim 10$  times higher than that for PVDF<sup>11</sup> but an elastic modulus of  $50\text{--}100$  GPa<sup>7</sup> and a maximum tensile strain of 0.2% before fracture.<sup>12</sup> Nanoribbons of PZT,<sup>5,13,14</sup> zinc oxide (ZnO),<sup>2,3</sup> or barium titanate ( $\text{BaTiO}_3$ )<sup>15,16</sup> printed onto stretchable elastomeric or flexible plastic substrates are thus susceptible to cracking, slipping, or delamination during operation.<sup>17,18</sup> Thus, despite their higher fundamental performances, these drawbacks naturally limit the

power generating capabilities of such hybrid devices, by requiring large forces to compress the materials and rendering the devices susceptible to mechanical failure.

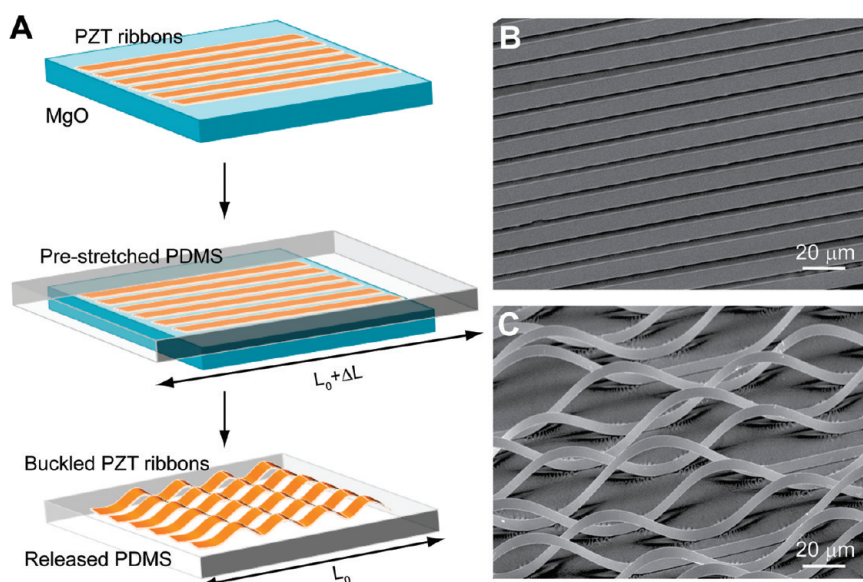
Here we present a new approach for the generation of hybrid energy harvesting materials, which can simultaneously display high piezoelectric performance while retaining mechanical integrity under both stretching and flexing operating modes. Inspired by recent work in rendering electronic materials stretchable,<sup>19–21</sup> our approach takes advantage of the nanoscale thicknesses of piezoelectric ribbons to rationally form wavy ribbon geometries on soft substrates, such as poly(dimethylsiloxane) (PDMS).<sup>19,22,23</sup> By utilizing prestrains in PDMS to buckle the ribbons, these structures can accommodate significantly higher compressive and tensile poststrains via changes in the wave amplitudes rather than destructive strains in the materials. Most importantly, localized probing of the buckled regions reveals enhanced piezoelectric response, allowing for the generation of stretchable energy harvesting devices.

Figure 1a illustrates our approach.<sup>5</sup> PZT ribbons ( $5\text{--}10$   $\mu\text{m}$  wide and  $250\text{--}500$  nm thick) were patterned on a magnesium oxide (MgO) host substrate as described previously<sup>5,13</sup> and subsequently released from the mother substrate using

**Received:** December 17, 2010

**Revised:** January 21, 2011

**Published:** February 15, 2011



**Figure 1.** Formation of wavy/buckled piezoelectric PZT ribbons. (a) From top to bottom: PZT ribbons were patterned on an MgO substrate and undercut etched to release them from the mother substrate; a slab of prestrained PDMS was laminated against the ribbons and peeled off quickly; retrieved PZT ribbons were transferred onto PDMS and formed wavy/buckled structures upon strain relaxation. (b) SEM image of PZT ribbons transfer printed to PDMS with zero prestrain. (c) PZT ribbons spontaneously buckled under prestrained conditions.

phosphoric acid (85% concentration, 75 °C, ~50 s). A slab of PDMS (~2 mm thick) was then elastically stretched and brought into conformal contact with the ribbons. Peeling off the PDMS allowed for complete transfer of the PZT ribbons to the elastomer via adhesive van der Waals forces in the surface-dominated ribbons. Finally, releasing the prestrain in the PDMS led to a compressive force in the PZT ribbons as the PDMS relaxed to zero strain, leading to periodic de-adhesion and buckling. The resulting wavy geometry is a result of the transfer of mechanical compressive energy into bending energy. Figure 1b shows a scanning electron microscopy (SEM) image of PZT ribbons transferred using unstrained PDMS, while Figure 1c shows PZT ribbons with a wavy/buckle structure induced by the prestrained PDMS.

The resulting geometry of the wavy/buckled ribbons is determined by several factors, including (1) the interaction between the PDMS and the ribbons, (2) the flexural rigidity of the PZT ribbons, and (3) the amount of prestrain in the compliant PDMS. For example, as seen from previous theoretical and experimental studies on ribbons,<sup>19,22,24,25</sup> a combination of small prestrain in PDMS and strong adhesion may not lead to buckling, since the ribbons remain in contact with the substrate. In contrast, PZT ribbons buckle due to the large prestrain and moderate to weak PZT/PDMS adhesion. The result is that originally flat ribbons of length  $L_0$  will adopt a sinusoidal buckling profile characterized by wavelength  $L$  and amplitude  $A$ , such that  $L_0$  becomes the contour length of the buckle. Supposing the relatively thick PDMS is completely relaxed,  $(L_0 - L)/L$  is then simply the prestrain from PDMS.

In order to estimate the wavelength and amplitude of the buckled regions, we consider the total energy in the system as the sum of the energy from the uniaxial strain in the ribbon and the energy due to bending,<sup>26</sup> adding an adhesion energy term between PZT ribbons and PDMS. Using an analytical method (see Supporting Information), the wave/buckle length and amplitude in periodic structures can be calculated by minimizing

the total energy, resulting in

$$L = \frac{\pi h}{\left[ \frac{\epsilon_{\text{pre}}}{1 + \epsilon_{\text{pre}}} - \sqrt{\left( \frac{\epsilon_{\text{pre}}}{1 + \epsilon_{\text{pre}}} \right)^2 - \frac{6w_{\text{ad}}}{Eh}} \right]^{0.5}} \quad (1)$$

$$A = \frac{2L_0}{\pi} \sqrt{\frac{\epsilon_{\text{pre}}}{1 + \epsilon_{\text{pre}}} - \frac{\pi^2 h^2}{3L_0^2}} \quad (2)$$

Here,  $h$  is the thickness of PZT ribbons,  $w_{\text{ad}}$  is the adhesion energy per unit area between the PZT and PDMS,  $E$  is the Young's modulus of PZT, and  $\epsilon_{\text{pre}}$  is the prestrain of PDMS.

In practice, variations in the ribbon thickness, the adhesive force, and the strain restoration could cause the ribbons to form aperiodic structures containing buckles with long intervening flat regions. For example, Figure 2a shows buckled PZT ribbons under high (8%, top image) and low (2%, bottom image) prestrain conditions. These results support the idea that larger prestrains lead to more periodic structures, with smaller prestrains yielding isolated buckles. Panels b and c of Figure 2 show experimental wavelength  $L$  and amplitude  $A$  data points, respectively, overlaid on curves calculated using the preceding equations for ribbon thicknesses of 250 and 500 nm. Notably, the experimental data agree well with the calculations using parameters  $E = 71$  GPa and  $w_{\text{ad}} = 0.12$  N/m, particularly when the prestrain is large. When  $\epsilon_{\text{pre}} \leq 0.02$ , the measured wavelength and amplitude are larger than the calculated value, due to the existence of long flat, unbuckled regions, indicating that at low prestrains the hybrid adhered state is lower in energy. Future work will allow us to control the geometry of the buckling more rigorously by, for example, chemical patterning of the PDMS stamp to define adhesion areas.<sup>27</sup>

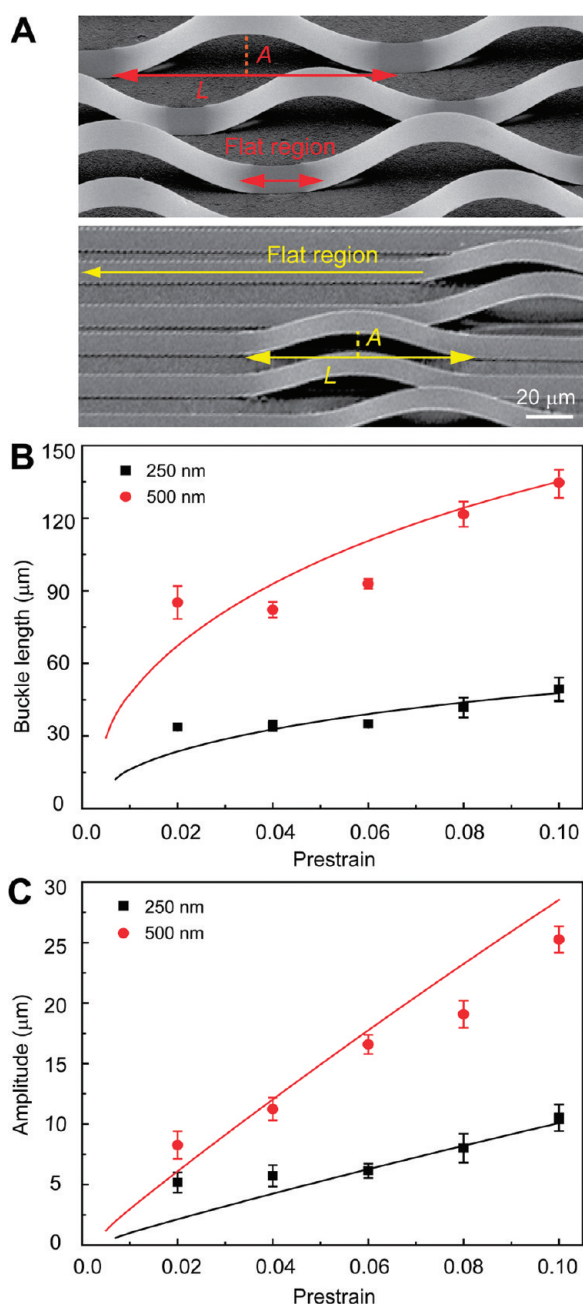


**Figure 2.** Engineering wavy ribbon geometry via prestrain. (a) Top: SEM image of wavy/buckled ribbons formed with large PDMS prestrain (8%). Bottom: SEM image of wavy/buckled ribbons formed with small PDMS prestrain (2%). (b, c) Experimental data and calculated fitting lines (from eqs 1 and 2) describing the buckle wavelength (b) and amplitude (c) as a function of various prestrains (black, 250 nm thick ribbons; red, 500 nm thick). A total of 10 data sets were used for the statistical analysis.

A key question is whether PZT ribbons formed using pre-stretched elastomers are capable of sustaining larger tensile strains due to their wavy/buckled geometry. To test this stretchability, hybrid structures containing flat ribbons and wavy/buckled PZT ribbons were sequentially mounted on a tensile stage and observed by SEM in situ during deformation. Figure 3 shows the results. For PDMS containing flat PZT ribbons, fracture initiated almost immediately with a low applied tensile strain (<1%) and propagated

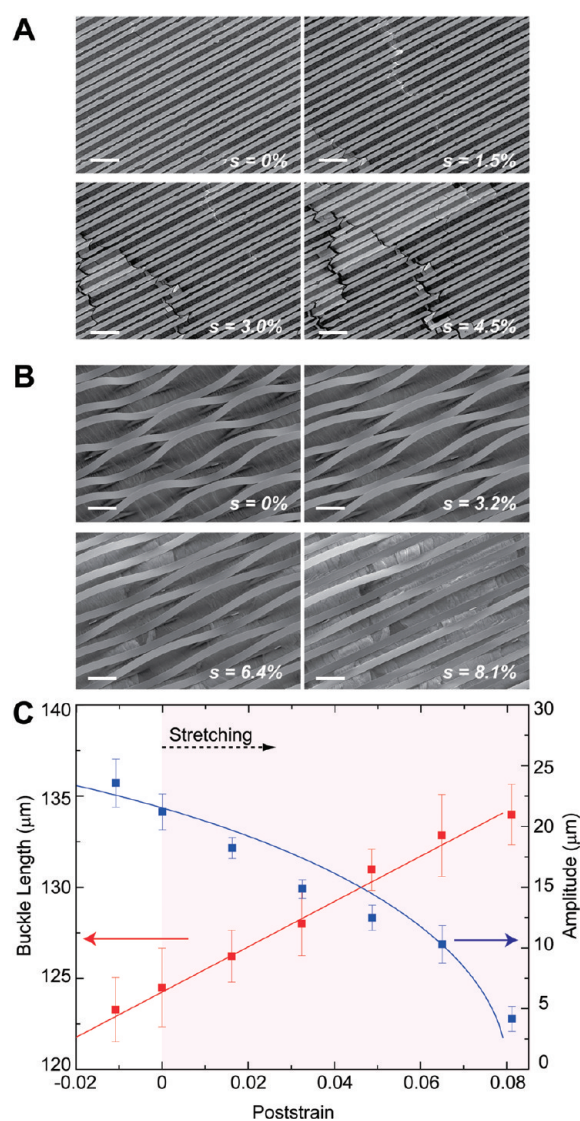


**Figure 3.** Application of tensile and compressive poststrains. (a, b) SEM images showing the stretching of flat ribbons (a) and wavy/buckled ribbons (b) on PDMS under progressive tensile strains. Scale bars: 20  $\mu\text{m}$ . (c) Plots of the change in wavelength and amplitude of buckled ribbons as a function of applied compressive or tensile poststrains. The red line is a linear fit of the experimental wavelength data, while the blue line is calculated from eq 2.

quickly into brittle fracture (Figure 3a), consistent with PZT's bulk failure strain of  $\sim 0.2\%$ .<sup>12</sup> By contrast, similar experiments on wavy/buckled PZT ribbons formed using an 8% prestrain do not show any stress cracks with applied tensile poststrains (up to >8%) and even under compressive strains ( $-1\%$ ) (Figure 3b). The stretch and release process was repeated for several cycles without observing any crack formation.

This stretchability is enabled by the ability of the wavy/buckled PZT ribbons to vary their wavelength and amplitude to accommodate an applied poststrain. Figure 3c shows the length and amplitude of the buckles with a range of applied poststrains. The initial wavelength and amplitude were 150 and 18  $\mu\text{m}$ , respectively. With increased poststrain, the wavelength increases linearly with as shown by the red data fit line, until the applied poststrain reaches the prestrain value, at which point ribbon slippage occurs. With compressive strains, slippage

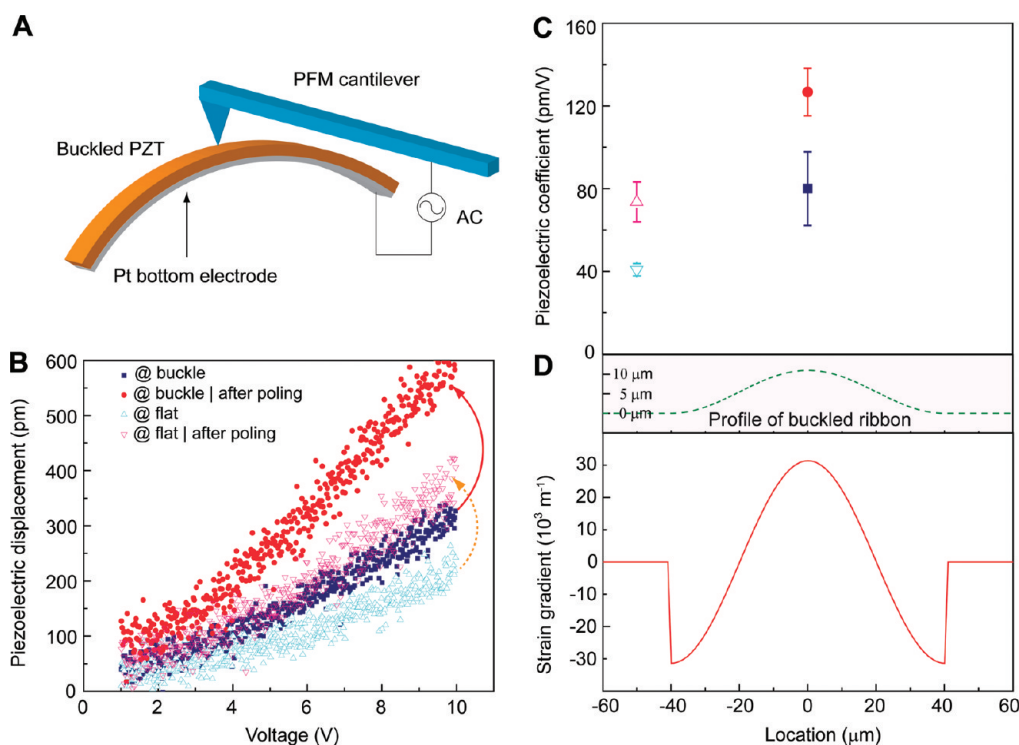


**Figure 4.** Local probing of piezoelectric response in buckled ribbons. (a) Schematic illustration of the PFM measurement performed on a ribbon buckle. (b) Representative piezoelectric displacement in buckled and flat regions of wavy PZT ribbons, as functions of the applied ac tip bias, before and after poling. (c) Average piezoelectric coefficients  $d_{33}$  retrieved from the PFM line slopes, before and after poling, and at various locations. Five sets of measurements from different buckles were used for the statistical analysis. (d) Calculated profile of a buckled ribbon and the corresponding strain gradient as determined from eq 4.

commences at a relatively smaller strain due to the large modulus of PZT and the increased bending energy. Similarly, the amplitude decreases with increased poststrain in order to maintain a constant ribbon contour length with changing wavelength. This amplitude can be calculated from eq 2 by substituting  $\varepsilon_{\text{pre}}$  with  $\varepsilon_{\text{pre}} - \varepsilon_{\text{post}}$ , as shown by the blue line in Figure 3c. In other words, imposing a poststrain  $\varepsilon_{\text{post}}$  on ribbons formed with a prestrain  $\varepsilon_{\text{pre}}$  yields equivalent geometries to ribbons released from a  $\varepsilon_{\text{pre}} - \varepsilon_{\text{post}}$  prestrain, as shown by the strong agreement between the data points and calculations.

Interestingly, in both the static and stretched states, fractures were not observed in the wavy/buckled ribbons even with the originally destructive tensile poststrain (up to 8%). This can be explained by the small residual strain present after ribbons relax into the wavy geometry. Following the preceding mechanical analysis, the uniaxial strain at the midplane of the ribbon is determined to be  $\varepsilon_{\text{mid}} = -4.5 \times 10^{-5}$ , which is 3 orders of magnitude smaller than the prestrain and remains a constant along the extent of the buckles. The maximum surface strain in PZT ribbons occurs at the peak and trough locations where the curvature is largest,  $\varepsilon_{\text{max}} = kh/2$ , where  $k$  is the curvature. Thus, for a ribbon thickness of 500 nm, and a prestrain of 8%, the calculated value of maximum surface strain is  $6.3 \times 10^{-3}$ , which is 1 order of magnitude smaller than the prestrain.

Previous studies on PZT thin films have suggested that in-plane tensile or compressive strains, either applied during measurement<sup>28</sup> or residual from the annealing procedure,<sup>29</sup> can significantly affect the piezoelectric response due to perovskite domain reorientation.<sup>30–32</sup> For example, a 45 MPa compressive stress in PZT films can lead to a 37% increase in piezoelectric displacement.<sup>29</sup> Another factor that may enhance

the piezoelectric response is strain gradient induced polarization, or the “flexoelectric” effect,<sup>33</sup> which is particularly prominent in thin films due to the larger strain gradients.<sup>34–36</sup> Finally, it has been shown that the substrate clamping effect can reduce the piezoelectric response of thick PZT films by up to 62% relative to bulk values of the piezoelectric charge constant,  $d_{33}$ .<sup>37</sup>

An intriguing question is whether the piezoelectric response is altered in buckled PZT ribbons relative to their flat counterparts. Piezoelectric force microscopy (PFM)<sup>38</sup> allows for local probing of the piezoelectric effect at various points along the ribbons, including at wavy and flat regions. Figure 4a shows the PFM experimental setup. Buckled PZT ribbons containing a Pt underlayer were generated with wavelengths of 80  $\mu\text{m}$  and heights of 11  $\mu\text{m}$ , and the PFM tip was brought into contact with the top of the ribbons. Next, an ac modulating voltage was applied between the tip and Pt underlayer, and the piezoelectric response amplitude was measured at the tip. Figure 4b shows the typical piezoelectric response amplitude as a function of applied ac voltage, as the modulating voltage was swept from 1 to 10 V. PFM measurements were performed at flat and buckled regions of the ribbons and were taken before and after poling at 100 kV/cm for 30 min. The piezoelectric coefficient,  $d_{33}$ , was determined from the slopes of the measured lines as described previously.<sup>5,39</sup> Figure 4c shows statistical  $d_{33}$  values taken from flat and buckled positions along the ribbons, before and after poling (10 V, 30 min). The data show that  $d_{33}$  values in the flat regions before and after poling are ca. 40 and 75 pm/V, respectively, while those in the buckled regions are ca. 80 and 130 pm/V, respectively. Significantly, this value of 130 pm/V is a 70% increase over the response at the flat region and thus represents the highest

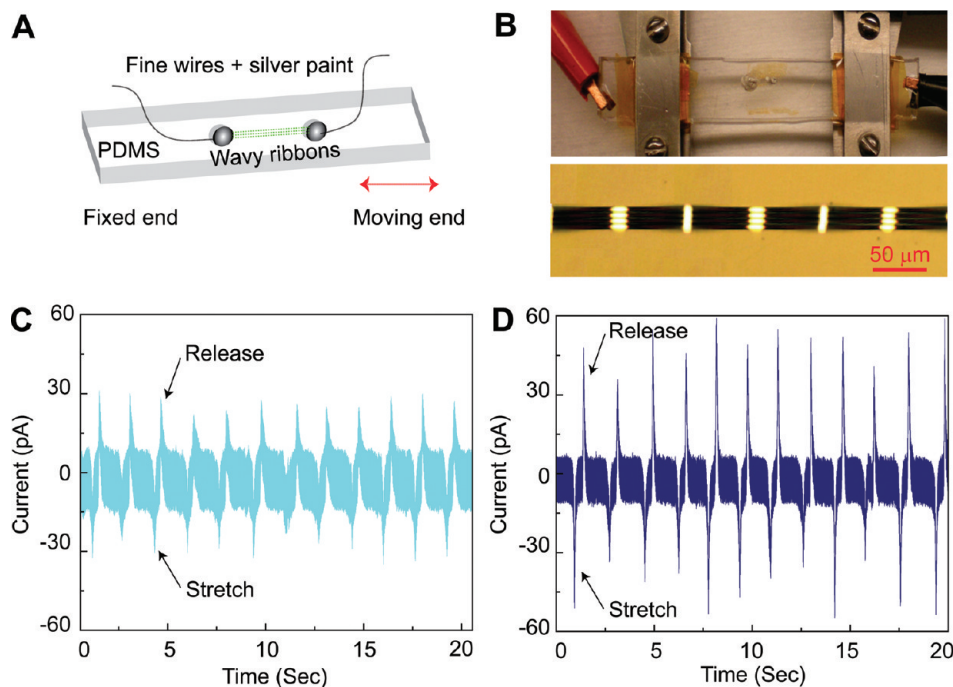


**Figure 5.** Energy conversion from stretching wavy/buckled PZT ribbons. (a) Schematic illustration of the experimental setup. (b) Top: photograph of the hybrid chip mounted on a stretching stage, with silver paint contacts separated by 0.5 mm. Bottom: optical micrograph of wavy ribbons bridging silver-paint contacts. (c, d) Short-circuit current measured from devices consisting of 5 (c) and 10 (d) ribbons under periodic stretch (8% strain) and release.

reported piezoelectric charge constant value on a flexible medium.<sup>5</sup>

To understand this piezoelectric enhancement, we calculated the uniaxial strain and strain gradient along the length of the wavy ribbons. The midplane uniaxial strain is given by

$$\varepsilon_{\text{mid}} = \frac{\pi^2 A^2}{4L_0^2} - \frac{\varepsilon_{\text{pre}}}{1 + \varepsilon_{\text{pre}}} \quad (3)$$

which yields a midplane stress of 8.5 MPa. This uniaxial strain is independent of the position, such that the midplane strain  $\varepsilon_{\text{mid}}$  and stress ( $\sigma_{\text{mid}} = E\varepsilon_{\text{mid}}$ ) are the same everywhere in the ribbons and are functions of prestrain only (since  $A$  and  $L_0$  are functions of prestrain only). Given the small magnitude of the uniaxial midplane strain, and the fact that it is a constant along the ribbons, we conclude that this strain does not account for the observed location-dependent enhancement. By contrast, in the buckled PZT ribbons, the strain gradient  $k$  is calculated as

$$k = -\frac{2\pi^2 A}{L_0^2} \cos\left(\frac{2\pi x}{L_0}\right) \quad (4)$$

which is a function of the location  $x$ . The strain gradient reaches positive and negative maxima at the peak and trough locations and is zero in flat ribbon regions. The maximum strain gradient can be as high as  $3.0 \times 10^4 \text{ m}^{-1}$ , which is several orders of magnitude larger than those achieved by four-point bend tests.<sup>34</sup> It can thus be concluded that this large, location-dependent strain gradient accounts for the piezoelectric enhancement. Further, the lack of substrate clamping in the elevated buckles is also expected to contribute to the increased piezoresponse.<sup>37</sup>

In order to demonstrate a proof-of-principle test of wavy piezoelectric ribbons in stretchable systems, the ribbons were integrated into energy conversion devices. PDMS samples

containing wavy/buckled ribbons were contacted by two spots of silver paint at the ribbon ends, connected to a current meter, poled at 10 kV/cm for 5 h, and mounted on a tensile stage for reversible stretching and releasing (strain  $\sim 0$ –8%). Figure 5a schematically illustrates the experimental setup, while Figure 5b shows the stretching stage and the ribbons under test, respectively. Peaks in the current signal were recorded at the moments of stretching and releasing, as indicated in panels c and d of Figure 5, which are from samples consisting of 5 wavy ribbons (effective cross-sectional area,  $A_{\text{cross}} \approx 12.5 \times 10^{-6} \text{ mm}^2$ ) and 10 wavy ribbons ( $A_{\text{cross}} \approx 25 \times 10^{-6} \text{ mm}^2$ ), respectively. On the basis of the current peaks, the current density is calculated to be  $j = I/A_{\text{cross}} \approx 2.5 \mu\text{A}/\text{mm}^2$ , which compares favorably to the peak current density measured in PZT nanowire-based devices.<sup>8,40</sup> The energy harvesting here is explained by overall changes in the midplane strain upon stretching and releasing, as described by eq 3.

In summary, nanothick ribbons of the piezoelectric ceramic PZT have been rendered stretchable via printing onto prestrained elastomeric substrates and releasing the strain to form buckled ribbons with engineered wavelengths and amplitudes. The wavy shapes of the ribbons can accommodate order-of-magnitude larger poststrains relative to their flat counterparts and thus are suitable for implementation in devices with challenging form factors. Further, the buckled ribbons display enhanced piezoelectric performance, thereby representing a promising hybrid materials platform for wearable or even implantable energy harvesting devices (using encapsulated PDMS).<sup>27</sup> Yet, a number of key challenges remain. In particular, future work will help us understand in more detail: (1) the relative contributions of substrate clamping and the flexoelectric effect enabled by the strain gradient to the enhanced piezoelectric response, (2) the ability to print buckled PZT ribbons over large areas, as has been

accomplished with flat ribbons, and (3) a better understanding of the hard inorganic/soft polymeric interface and its longevity under mechano-electrical cycling.

### ■ ASSOCIATED CONTENT

**S** **Supporting Information.** Detailed analytical method for deriving the buckle wavelengths and amplitudes. This material is available free of charge via the Internet at <http://pubs.acs.org>.

### ■ AUTHOR INFORMATION

#### Corresponding Author

\*E-mail: [mcm@princeton.edu](mailto:mcm@princeton.edu) and [purohit@seas.upenn.edu](mailto:purohit@seas.upenn.edu).

### ■ ACKNOWLEDGMENT

We acknowledge the use of the PRISM Imaging and Analysis Center, which is supported by the NSF MRSEC Program via the Princeton Center for Complex Materials (No. DMR-0819860). P.K.P. acknowledges support of this work by the National Science Foundation CAREER Award (No. CMMI-0953548). M.C.M. acknowledges support of this work by the Defense Advanced Research Projects Agency (No. N66001-10-1-2012) and the National Science Foundation (No. NSF CMMI-1036055).

### ■ REFERENCES

- (1) Service, R. F. *Science* **2010**, *328*, 304–305.
- (2) Xu, S.; Qin, Y.; Xu, C.; Wei, Y.; Yang, R.; Wang, Z. L. *Nat. Nanotechnol.* **2010**, *5*, 366–373.
- (3) Yang, R.; Qin, Y.; Dai, L.; Wang, Z. L. *Nat. Nanotechnol.* **2009**, *4*, 34–39.
- (4) Yang, R.; Qin, Y.; Li, C.; Zhu, G.; Wang, Z. L. *Nano Lett.* **2009**, *9*, 1201–1205.
- (5) Qi, Y.; Jafferis, N. T.; Lyons, K.; Lee, C. M.; Ahmad, H.; McAlpine, M. C. *Nano Lett.* **2010**, *10*, 524–528.
- (6) Qi, Y.; McAlpine, M. C. *Energy Environ. Sci.* **2010**, *3*, 1275–1285.
- (7) Starner, T. *IBM Syst. J.* **1996**, *35*, 618–629.
- (8) Xu, S.; Hansen, B. J.; Wang, Z. L. *Nat. Commun.* **2010**, *1*, 93.
- (9) Chang, C.; Tran, V. H.; Wang, J.; Fuh, Y.-K.; Lin, L. *Nano Lett.* **2010**, *10*, 726–731.
- (10) Furukawa, T.; Seo, N. *Jpn. J. Appl. Phys.* **1990**, *29*, 675–680.
- (11) Kim, H.; Tadesse, Y.; Priya, S. *Energy Harvesting Technologies*; Springer: New York, 2008.
- (12) Guillon, O.; Thiebaud, F.; Perreux, D. *Int. J. Fract.* **2002**, *117*, 235–246.
- (13) Nguyen, T. D.; Nagarah, J. M.; Qi, Y.; Nonnenmann, S. S.; Morozov, A. V.; Li, S.; Arnold, C. B.; McAlpine, M. C. *Nano Lett.* **2010**, *10*, 4595–4599.
- (14) Martin, C. R.; Aksay, I. A. *J. Phys. Chem. B* **2003**, *107*, 4261–4268.
- (15) Park, K.-I.; Xu, S.; Liu, Y.; Hwang, G.-T.; Kang, S.-J. L.; Wang, Z. L.; Lee, K. J. *Nano Lett.* **2010**, *10*, 4939–4943.
- (16) Spanier, J. E.; Kolpak, A. M.; Urban, J. J.; Grinberg, I.; Lian, O. Y.; Yun, W. S.; Rappe, A. M.; Park, H. *Nano Lett.* **2006**, *6*, 735–739.
- (17) Park, S. I.; Ahn, J. H.; Feng, X.; Wang, S. D.; Huang, Y. G.; Rogers, J. A. *Adv. Funct. Mater.* **2008**, *18*, 2673–2684.
- (18) Cho, J.-H.; Datta, D.; Park, S.-Y.; Shenoy, V. B.; Gracias, D. H. *Nano Lett.* **2010**, *10*, 5098–5102.
- (19) (a) Khang, D.-Y.; Jiang, H.; Huang, Y.; Rogers, J. A. *Science* **2006**, *311*, 208–212. (b) Sun, Y. G.; Kumar, V.; Adesida, I.; Rogers, J. A. *Adv. Mater.* **2006**, *18*, 2857–2862.
- (20) Sekitani, T.; Noguchi, Y.; Hata, K.; Fukushima, T.; Aida, T.; Someya, T. *Science* **2008**, *321*, 1468–1472.
- (21) Lacour, S. P.; Jones, J.; Wagner, S.; Li, T.; Suo, Z. *Proc. IEEE* **2005**, *93*, 1459–1467.
- (22) Bowden, N.; Brittain, S.; Evans, A. G.; Hutchinson, J. W.; Whitesides, G. M. *Nature* **1998**, *393*, 146–149.
- (23) Ko, H. C.; Baca, A. J.; Rogers, J. A. *Nano Lett.* **2006**, *6*, 2318–2324.
- (24) Song, J.; Jiang, H.; Liu, Z. J.; Khang, D. Y.; Huang, Y.; Rogers, J. A.; Lu, C.; Koh, C. G. *Int. J. Solids Struct.* **2008**, *45*, 3107–3121.
- (25) Xiao, J.; Carlson, A.; Liu, Z. J.; Huang, Y.; Rogers, J. A. *J. Appl. Mech.* **2010**, *77*, No. 011003.
- (26) Song, J.; Huang, Y.; Xiao, J.; Wang, S.; Hwang, K. C.; Ko, H. C.; Kim, D. H.; Stoykovich, M. P.; Rogers, J. A. *J. Appl. Phys.* **2009**, *105*, No. 123516.
- (27) Sun, Y.; Choi, W. M.; Jiang, H.; Huang, Y. Y.; Rogers, J. A. *Nat. Nanotechnol.* **2006**, *1*, 201–207.
- (28) Rossetti, J.; George, A.; Cross, L. E.; Kushida, K. *Appl. Phys. Lett.* **1991**, *59*, 2524–2526.
- (29) Lee, J. W.; Lee, S. M.; Park, C. S.; Park, G. T.; Kim, H. E. *J. Sol-Gel Sci. Technol.* **2007**, *42*, 305–308.
- (30) Lu, X. M.; Zhu, J. S.; Li, X. L.; Zhang, Z. G.; Zhang, X. S.; Wu, D.; Yan, F.; Ding, Y.; Wang, Y. *Appl. Phys. Lett.* **2000**, *76*, 3103–3105.
- (31) Kumazawa, T.; Kumagai, Y.; Miura, H.; Kitano, M.; Kushida, K. *Appl. Phys. Lett.* **1998**, *72*, 608–610.
- (32) Kelman, M. B.; McIntyre, P. C.; Hendrix, B. C.; Bilodeau, S. M.; Roeder, J. F. *J. Appl. Phys.* **2003**, *93*, 9231–9236.
- (33) Ma, W.; Cross, L. E. *Appl. Phys. Lett.* **2005**, *86*, No. 072905.
- (34) Ma, W. H.; Cross, L. E. *Appl. Phys. Lett.* **2003**, *82*, 3293–3295.
- (35) Majdoub, M. S.; Sharma, P.; Cagin, T. *Phys. Rev. B* **2008**, *77*, No. 125424.
- (36) Nonnenmann, S. S.; Leaffer, O. D.; Gallo, E. M.; Coster, M. T.; Spanier, J. E. *Nano Lett.* **2010**, *10*, 542–546.
- (37) Torah, R. N.; Beeby, S. P.; White, N. M. *J. Phys. D: Appl. Phys.* **2004**, *37*, 1074–1078.
- (38) Bonnell, D. A.; Kalinin, S. V.; Kholkin, A. L.; Gruverman, A. *MRS Bull.* **2009**, *34*, 648–657.
- (39) Kalinin, S. V.; Bonnell, D. A. *Phys. Rev. B* **2002**, *65*, No. 125408.
- (40) Chen, X.; Xu, S.; Yao, N.; Shi, Y. *Nano Lett.* **2010**, *10*, 2133–2137.